Energy-Level Alignment at the Organic/Electrode Interface in Organic Optoelectronic Devices

Zhanhao Hu, Zhiming Zhong, Yawen Chen, Chen Sun, Fei Huang, Junbiao Peng, Jian Wang, and Yong Cao*

It is commonly believed that the work-function reduction effect of the cathode interfacial material in organic electronic devices leads to better energy-level alignment at the organic/electrode interface, which enhances the device performance. However, there is no agreement on the exact dipole direction in the literature. In this study, a peel-off method to reveal the buried organic/metal interface to examine the energy-level alignment is developed. By splitting the device at different interfaces, it is discovered that oppositely oriented dipoles are formed at different surfaces of the interfacial layer. Moreover, the function of the electrode interface differs in different device types. In organic light-emitting diodes, the vacuum-level alignment generally occurs at the organic/cathode interface, while in organic photovoltaic devices, the Fermi-level pinning commonly happens. Both are determined by the integer charge-transfer levels of the organic materials and the work-function of the electrode. As a result, the performance enhancement by the cathode interfacial material in organic photovoltaic devices cannot be solely explained by the energy-level alignment. The clarification of the energy-level alignment not only helps understand the device operation but also sets up a guideline to design the devices with better performance.

1. Introduction

Organic semiconductors (OSCs) since their birth have been extensively studied and applied in various electronic devices owing to the unique properties compared to their inorganic counterparts.[1–3] Almost all organic devices are thin-film multilayer devices, like organic light-emitting diodes (OLEDs) and organic photovoltaics (OPVs), in which the organic layers are the functional layers while the metal layers are the electrodes. Therefore, organic/organic and organic/metal interfaces are crucial in improving device performance.[4,5]

It is well known that a limiting factor preventing the practical application of OSC lies in the use of low work-function (WF) metal as the cathode in OLEDs and OPVs, which is sensitive to moisture and oxygen.[6,7] To address this problem, a class of cathode interfacial material (CIM), usually an organic electrolyte or inorganic salt, has been developed to enable the utilization of more stable high WF conductors like Au, Ag, Al and indium tin oxide (ITO).[8–11] The key molecular structure of the CIM is the polar component.[10,11] It is believed that the CIM layer introduces an interfacial dipole at the organic/metal interface to reduce the effective WF of the metal, leading to better energy-level alignment to enhance the device performance.

However, there is no agreement in the literatures in regard to the direction of the vacuum-level shift caused by the CIM dipole layer, particularly in devices with a regular device architecture (substrate/anode/organic/cathode). The confusion comes from the specific sample structure employed in the surface potential measurement. To characterize the WF modification effects of CIMs, the most common techniques are the ultraviolet photoelectron spectroscopy (UPS) and the Kelvin probe (KP). Two sample configurations are generally used. One is CIM layer on top of the predeposited cathode metal[12–16] as illustrated in **Figure 1**a. The other is CIM layer on top of the organic active layer[17–20] as shown in Figure 1b. Generally, the surface potential measurement on the CIM exhibits a decreased WF with respect to the substrates for both sample configurations. As a result, the proposed CIM dipole directions are opposite to each other when the measurement results are directly transferred into a complete device. As shown in Figure 1, the measurement of the CIM on top of the metal gives a negative dipole direction (defined as that from cathode to anode) which lifts the vacuum level of the metal, while the measurement of the CIM on top of the active layer gives an positive dipole direction (defined as that from anode to cathode) which lowers the vacuum level of the metal. Unfortunately, without further investigation, both are adopted in the interpretation of the CIM's role in a complete device, and the contradiction has yet to be addressed in any report so far.

The controversy on the dipole direction is the consequence of only considering one interface of the CIM layer, i.e., either the CIM/metal interface or the active layer/CIM interface. Without taking into account both interfaces, the complete energy-level alignment across the CIM layer cannot be correctly determined.

Dr. Z. Hu, Dr. Z. Zhong, Dr. Y. Chen, Dr. C. Sun, Prof. F. Huang, Prof. J. Peng, Prof. J. Wang, Prof. Y. Cao
Institute of Polymer Optoelectronic Materials and Devices
State Key Laboratory of Luminescent Materials and Devices
South China University of Technology
Guangzhou 510640, P. R. China
E-mail: jianwang@scut.edu.cn

DOI: 10.1002/adfm.201503420

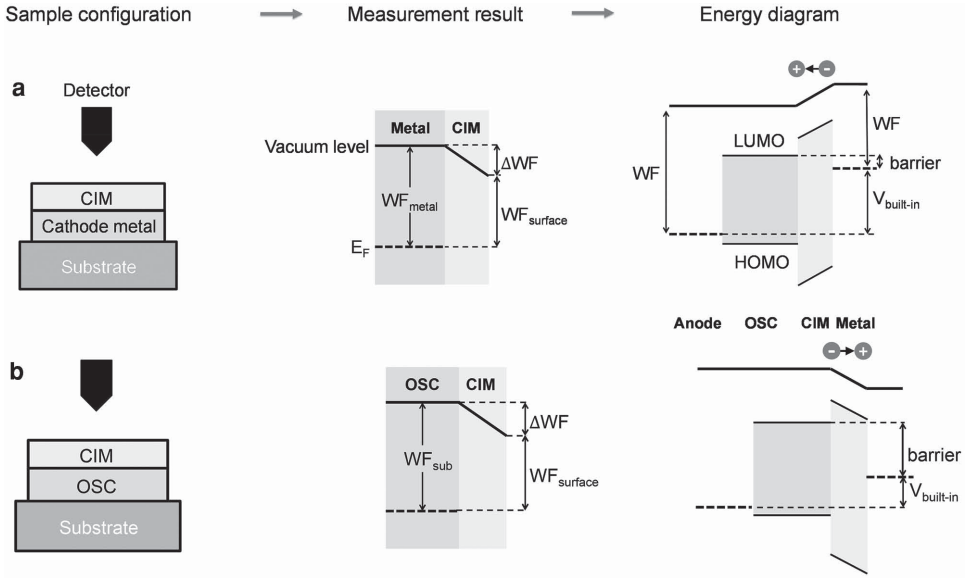

Figure 1. a) With CIM on the predeposited metal layer, the interfacial dipole's direction is from cathode to anode which elevates the vacuum level on the metal side. b) With CIM on the organic semiconductor layer, the interfacial dipole's direction is from anode to cathode which lowers the vacuum level on the metal side.

Moreover, in an actual regular device, the metal is thermally evaporated onto the CIM. Due to the strong interaction between the metal and CIM, the CIM's dipole is not necessarily to keep its original direction after metal deposition, which cannot be detected in conventional measurements with the predeposited metal/CIM configuration.[21,22] Thus, a better measurement technique should be developed to probe inside the CIM/postdeposited metal interface in order to determine the correct dipole direction.

In our contribution, we have developed a peel-off method to expose the buried organic/metal interface. By carefully studying the energy alignment at each interface, it is discovered that two oppositely oriented dipoles are formed at the different surfaces of the CIM layer. Taking both CIM interfaces into account, energetic diagrams of the OLED and OPV devices are clarified. In OLED devices, the vacuum level is aligned across the organic/cathode interface. The vacuum-level alignment (VLA) reduces the electron injection barrier, leading to better device performance. In OPV devices, the cathode WF is pinned to the fullerene. Therefore, from the perspective of energy-level alignment, the modification of poly[(9,9-bis(3′-(*N*,*N*-dimethylamino)-propyl)-2,7-fluorene)-alt-2,7-(9,9-dioctylfluorene)] (PFN) does not introduce any significant change to the device.

2. Results and Discussion

2.1. Peel-Off Method

In our work, the water/alcohol-soluble-conjugated polymer electrolyte, PFN, is selected as a representative CIM (for chemical structures see Figure S1 in the Supporting Information). Like other reported CIMs, PFN has a polar side chain (aliphatic amine) that gives rise to its WF modification function on many electrode materials.[11,23] OLED and OPV devices incorporating PFN have achieved high efficiencies in both regular and inverted device structures.[8,17,24–26] Al is chosen as the cathode metal in the devices.

For surface potential measurement, a KP instrument in a nitrogen-filled glovebox is employed. The WF value is derived from the contact potential difference, calibrated by the highly oriented pyrolytic graphite (for KP operation see Figure S2 in the Supporting Information). To enable direct WF characterization on the buried interfaces inside the device, a peel-off method has been developed. Since the samples are split from the complete device by peeling-off, the measured surface WF on the interface is a real representative of the energy-level alignment in the actual device. The measurements reveal that there are two different interactions between PFN and the active layer, and between PFN and metal, which lead to oppositely oriented dipoles at organic/organic and organic/metal interfaces, of which the strengths depend on the specific materials in contact.

The peel-off method is schematically illustrated in **Figure 2**. After the fabrication of the device with ITO anode and Al cathode, the ITO surface of another ITO glass is adhered to the Al surface through a double-sided conducting tape. The device is split into two halves manually. Through control of the adhesion of the interfaces, either the cathode stack (Procedure 1) or the active layer/cathode stack (Procedure 2) can be selectively detached. The exposed interfaces of the peeled-off samples are subsequently characterized by the KP. While the cathode stack from Procedure 1 enables direct measurement of the dipole at the organic/metal interface, the active layer/cathode stack from Procedure 2 takes into account both the organic/metal and organic/organic dipoles plus energy-level shift within the active layer.

2.2. Energy-Level Alignment in OLED

The OLED devices are fabricated with poly[2-methoxy-5-(2′-ethylhexyloxy)-*p*-phenylene vinylene] (MEH-PPV) as the

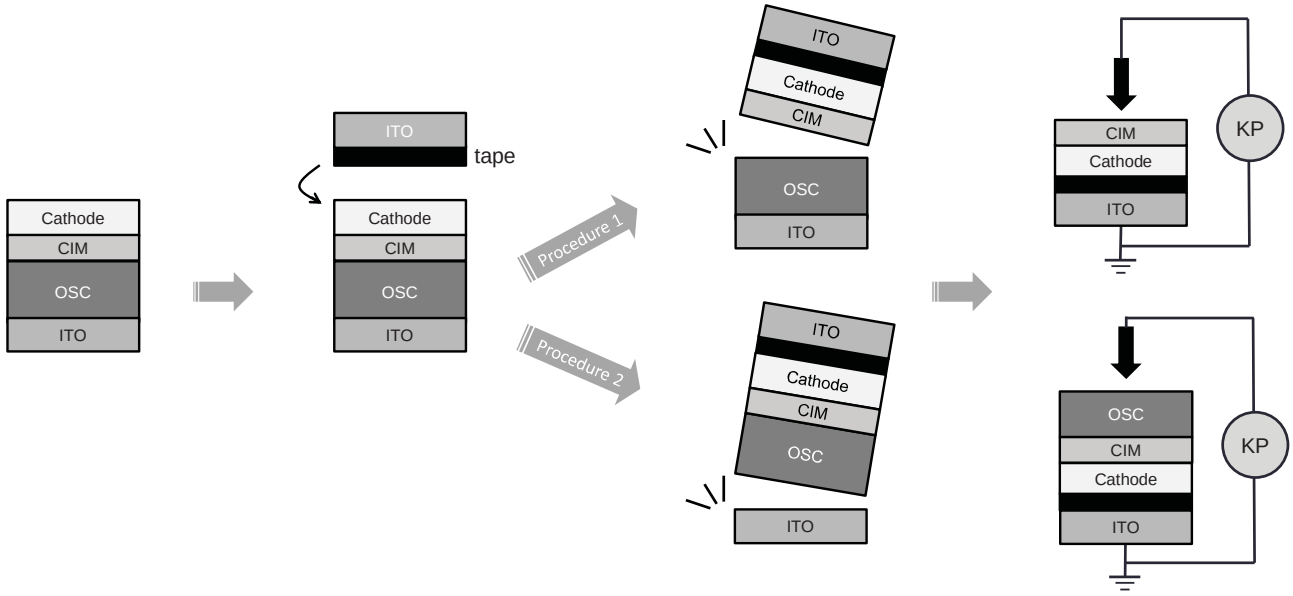

Figure 2. The schematic illustration of the peel-off method. Two procedures are adopted for the selective peeling at the desired interfaces by tuning the interface adhesion. Thus, a CIM/cathode stack or OSC/CIM/cathode stack is obtained and flipped over for the WF measurement by the KP.

light-emitting layer. The WFs on each layer immediately after deposition during device fabrication, and the WFs on the peeled-off samples are presented in **Figure 3**a. The WF of the ITO/MEH-PPV substrate is around 4.7 eV. Spin-coating PFN on the ITO/MEH-PPV substrate causes a 0.1 eV WF reduction, suggesting that there is a weak dipole at the MEH-PPV/PFN interface, probably arising from the hydrophobic MEH-PPV surface which induces a preferential orientation of the amino side chains of PFN.[27] Other mechanisms, such as image charge effect and partially protonated amines, were also proposed.[23,28] On the peeled-off sample, the WF of ITO/MEH-PPV~ (~ denotes the split interface) is as same as that of the ITO/MEH-PPV substrate, showing that PFN is completely removed from MEH-PPV surface after the peeling-off procedure.

The WF of low-vacuum-deposited (≈10^{-4} Pa) Al is around 3.3 eV. The spontaneous oxidation of the Al surface makes Al WF smaller than the UPS value.[4,5] After PFN is spin-coated on Al, the WF is reduced to 3.1 eV, indicating that a new dipole layer is formed at the PFN/Al interface. In comparison, the peeled-off ~PFN/Al reveals a WF of about 3.0 eV, confirming the formation of the new dipole layer at the PFN/Al interface. It is believed that the dipole comes from the Lewis acid–base interaction in which the lone pair electrons from amine is partially transferred to the metal.[11,29,30] During thermal evaporation process, high energy Al atoms diffuse into the CIM layer, creating stronger dipoles (Figure 3 inset). As a result, the WF of peeled off ~PFN/Al is smaller than that of Al/PFN in which PFN is directly spin-coated on the predeposited Al substrate. Moreover, it is reported that if the evaporated metal atoms diffuse through the self-assembled monolayer CIM, and reach the semiconductor/CIM interface, the strong interaction between CIM and metal can even cause an inversion of the dipole formerly formed before metal deposition.[31] In the studied OLED devices, the PFN layer on top of MEH-PPV is 20 nm thick, which suggests the possibility of the coexistence of two oppositely oriented dipoles at different interfaces of PFN. As shown earlier, PFN is totally removed from MEH-PPV by the peeling-off procedure. Thus, a simultaneous observation of two dipoles can only be achieved by employing the peeling-off Procedure 2, which leaves both PFN interfaces intact.

To achieve the selective peeling-off at the ITO/MEH-PPV interface, a cross-linkable PFN derivative PFN-OX (Figure S1, Supporting Information) with almost identical WF modification effect is used.[32,33] The cross-linking at moderate temperature gives a better adhesion between MEH-PPV and PFN than that between MEH-PPV and ITO. A reference OLED device with the structure of ITO/MEH-PPV/Al is also made and split to expose the ITO~MEH-PPV/Al interface. Without PFN layer, the WF of ~MEH-PPV/Al is around 3.3 eV, equal to the WF of predeposited Al. With PFN layer, the WF of ~MEH-PPV/PFN/Al is about 3.1 eV, showing a net dipole of negative 0.2 eV. Combining the 3.0 eV WF of ~PFN/Al and the weak dipole at the MEH-PPV/PFN interface, we propose that there are two oppositely oriented dipoles at different PFN interfaces. A negative dipole of 0.3 eV exists at the PFN/Al interface, while a positive dipole of 0.1 eV exists at the MEH-PPV/PFN interface. Therefore, the net dipole is negative 0.2 eV. The energy-level alignment across various interfaces are schematically illustrated in Figure 3a.

Furthermore, to simultaneously observe the coexistence of oppositely oriented dipoles at different PFN surfaces, an ITO/PFN/Al device is split. Since the PFN layer is strongly adhered to both ITO and Al, the separation occurs inside the PFN layer. By measuring the WF change at ITO/PFN~ and ~PFN/Al, the coexistence of the two dipoles in PFN is directly verified (Figure S4, Supporting Information).

2.3. Energy-Level Alignment in OPV

In OPV devices, fullerenes with large electron affinity are commonly used as the electron-accepting material. Recently, strong

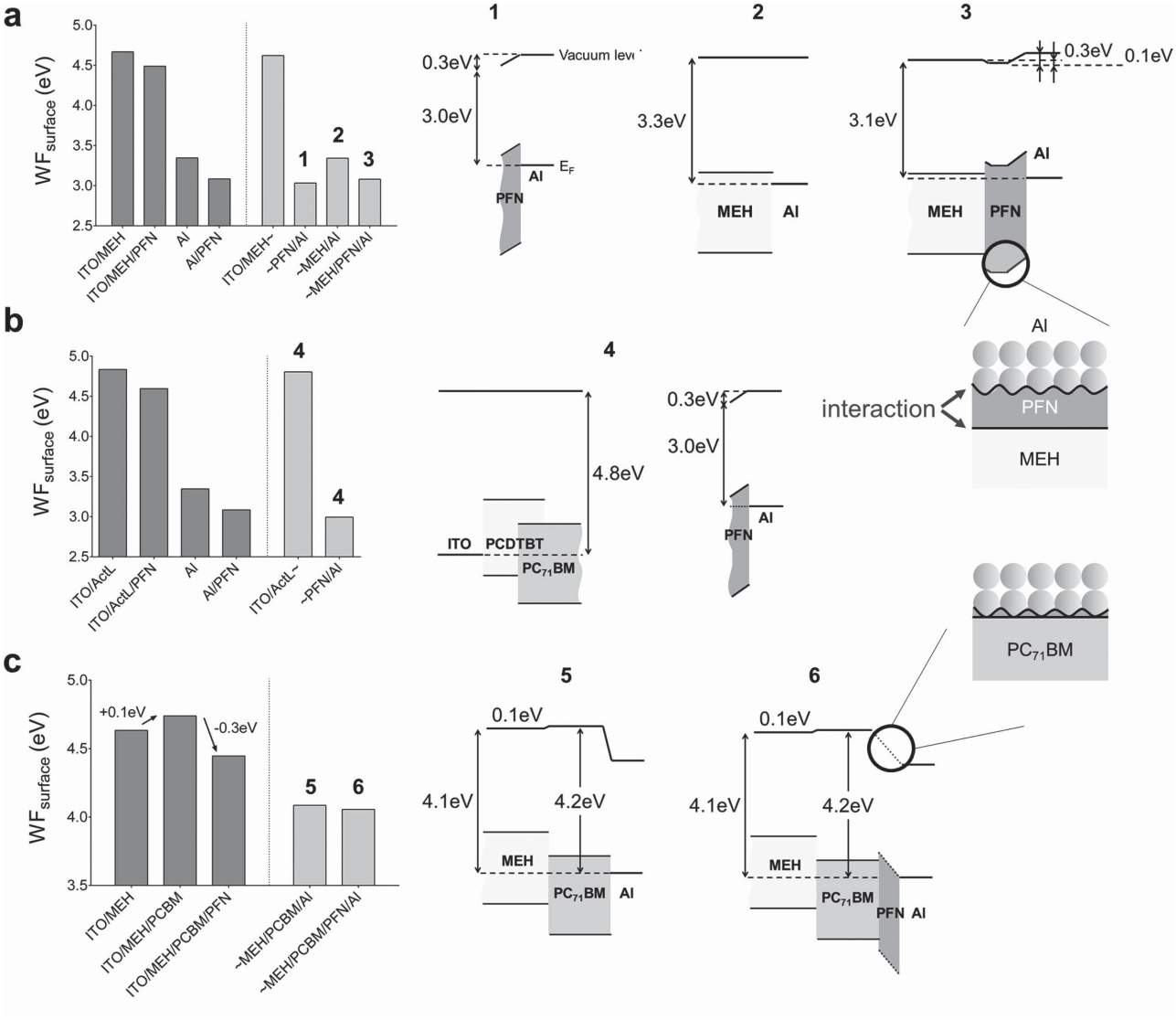

Figure 3. The surface WF on each layer during device fabrication and on the peeled-off samples. The left panel shows data of a) the OLED device in the configuration of ITO/MEH-PPV/Al with and without PFN, b) bulk heterojunction OPV device in the configuration of ITO/PCDTBT:PC71BM/PFN/Al, and c) bilayer OPV device in the configuration of ITO/MEH-PPV/PC71BM/Al with and without PFN. The right panel shows the corresponding energy diagrams of the peeled-off samples. In the OLED device (a), two dipole layers with opposite direction coexist on different PFN surfaces. In the OPV device (c), energy-level pinning occurs at the fullerene/PFN/Al interface.

interactions between PFN (or PFN-like CIMs with electron-donating functionality) and fullerene were discovered.[34–36] To study the energy-level alignment in OPV, a typical device of ITO/poly[*N*-9″-hepta-decanyl-2,7-carbazole-*alt*-5,5-(4′,7′-di-2-thienyl-2′,1′,3′-benzothiadiazole) (PCDTBT): [6,6]-phenyl C71-butyric acid methyl ester ($PC_{71}BM$)/PFN/Al is fabricated. As shown in Figure 3b, after PFN is spin-coated on the active layer, the WF is lowed by about 0.3 eV consistent with other reports.[17,30] The WF reduction mainly comes from the interaction between PFN and fullerene, since spin-coating PFN on pure $PC_{71}BM$ film reduces the WF by 0.4 eV, while on pure PCDTBT reduces the WF by only 0.06 eV. On the peeled-off samples, the WF of ITO/PCDTBT:$PC_{71}BM$~ is identical to that of ITO/PCDTBT:$PC_{71}BM$, indicating that PFN is completely removed from the active layer by the peeling-off process. The WF of ~PFN/Al is found to be about 3.0 eV, suggesting a new dipole formed at the PFN/Al interface as the case in the OLED device. The energy-level alignment across the ITO/active layer~ and ~PFN/Al is illustrated in Figure 3b. Since PFN is totally removed from the active layer on the peeled-off sample, it is unknown whether the dipole at the PCDTBT:$PC_{71}BM$/PFN interface is maintained after the PFN/Al dipole is formed. Similar to the investigation on the OLED device, the OPV device should be split at the ITO/active layer to leave both interfaces of PFN intact.

Unfortunately, due to the strong adhesion of the active layer to the ITO substrate, the device cannot be split at the ITO/active layer. To solve the problem, bilayer devices in the configuration of ITO/MEH-PPV/$PC_{71}BM$/Al and ITO/MEH-PPV/$PC_{71}BM$/PFN/Al are fabricated. The bilayer devices can be

easily separated at the ITO/MEH-PPV interface because of the weaker adhesion of MEH-PPV to ITO. As shown earlier, since the fullerene component dominates the interfacial energetics in the bulk heterojunction device, the energy alignment in the bilayer device should be applicable to the bulk heterojunction device. The WF pinning study of various materials in the following section verifies that the energy alignment in the bilayer device is consistent with that in the bulk heterojunction device, due to the low-integer charge-transfer level of the fullerene.

The WF evolution through the device fabrication and the WF of the peeled-off samples are illustrated in Figure 3c. It is found that $PC_{71}BM$ on top of MEH-PPV increases the WF by 0.1 eV. The negative dipole comes from the electron transfer from MEH-PPV to $PC_{71}BM$ at the interface.[37] Further deposition of PFN on $PC_{71}BM$ leads to a 0.3 eV reduction. For the peeled-off samples, both ~MEH-PPV/$PC_{71}BM$/Al and ~MEH-PPV/$PC_{71}BM$/PFN/Al show a WF of about 4.1 eV. Adding the 0.1 eV upshift at the MEH-PPV/$PC_{71}BM$ interface, the effective WF of both $PC_{71}BM$/Al and $PC_{71}BM$/PFN/Al are 4.2 eV. The same surface WFs imply that the cathode Fermi level is pinned by the $PC_{71}BM$ layer. On the samples in which the layers are deposited in reverse sequence on predeposited Al, the same surface WF of Al/$PC_{71}PM$, Al/PFN/$PC_{71}BM$, Al/PCDTBT:$PC_{71}BM$ and Al/PFN/PCDTBT:$PC_{71}BM$ confirms the WF pinning (Figure S5, Supporting Information). Similar results were also observed by UPS in other reports.[13,16,38] In device studies, the open-circuit voltage independent of the cathode WF indicates the energy pinning, too.[39]

Because of the energy-level pinning, the information about the PFN dipole direction at different PFN interfaces is screened. The thickness of the PFN layer in OPV devices is only around 5 nm,[17,33] which makes the Al diffusion possible.

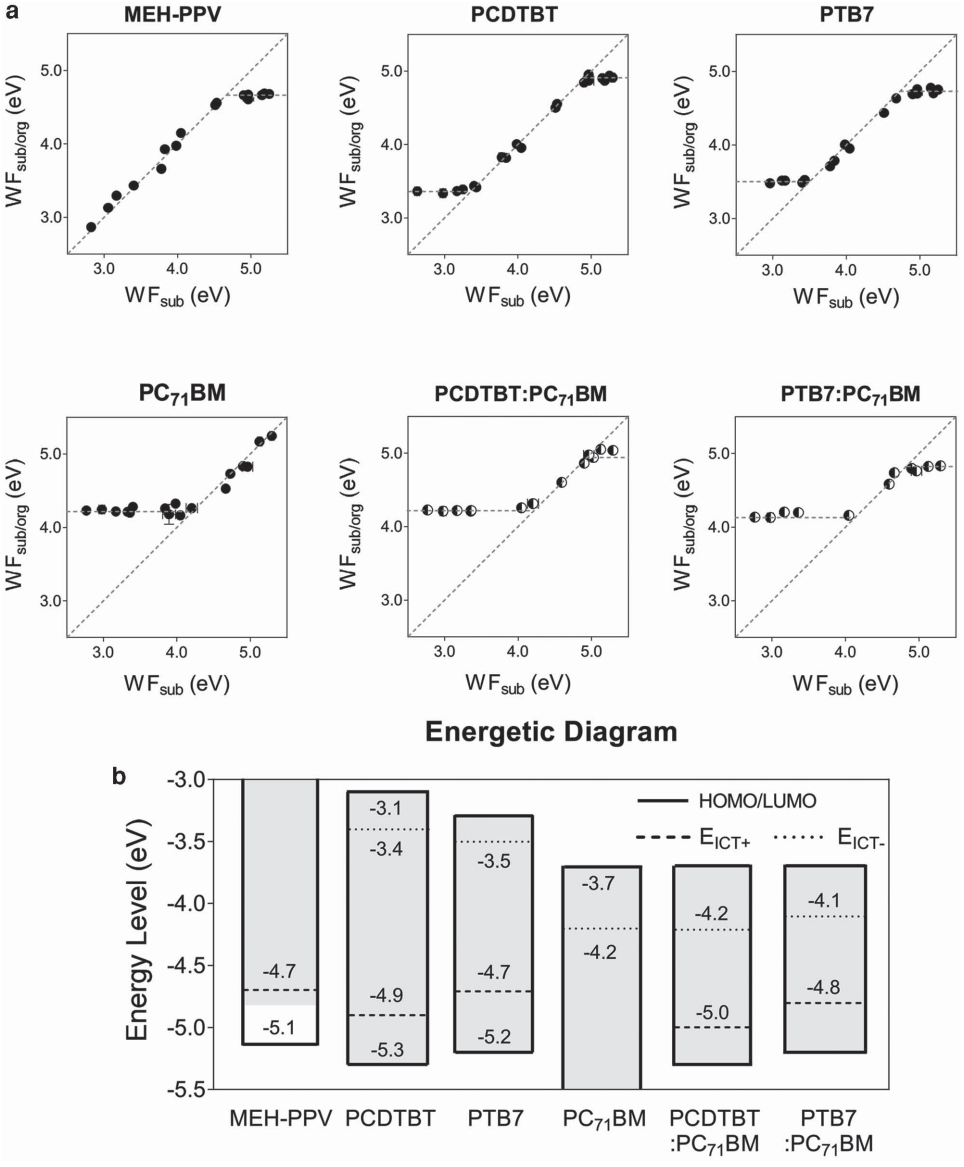

Figure 4. The ICT levels of some common active layer materials. a) Plots of the surface WF versus the substrate WF. b) The summary of the measured ICT levels together with both HOMO and LUMO levels from the literatures.[26,41,42]

Therefore, the active layer/PFN interface and PFN/Al interface mix together, and there are two interactions, namely amines to fullerene and amines to Al (Figure 3 inset), competing against each other at the PFN interface. In some areas, the amine–fullerene interaction dominates, while in other areas, the amine–Al interaction dominates. Nonetheless, the net vacuum-level shift at the PFN interface in the OPV device is about 0.9 eV due to the WF pinning as depicted in Figure 3c.

2.4. Integer Charge Transfer

The electrode WF pinning effect at organic/organic and organic/metal interfaces can be well explained by the ICT model.[4] The model proposes two energy levels in the bandgap of an OSC, i.e., the ICT states of holes (E_{ICT+}) and electrons (E_{ICT-}) which represent the smallest energies required to oxidize or reduce the organic at the interface. The energy-level alignment across the interface is determined by the relative position of the ICT levels of the organic materials and the Fermi level of the electrode. Here, the ICT levels of MEH-PPV, PCDTBT, $PC_{71}BM$, as well as the recent high-performance donor thieno[3,4-b]thiophene/benzodithiophene (PTB7), along with their blended films, were systematically measured. By depositing the organic layer on substrates whose WF covers a large range, the ICT levels can be identified from the plot of the surface WF versus substrate WF as shown in **Figure 4**a. It is found that for substrate WF between E_{ICT+} and E_{ICT-}, the plots have a line slope = 1, indicating the VLA. When the substrate WF moves outside the E_{ICT+} and E_{ICT-} range, WF pinning is observed where the ICT levels can be determined. The ICT levels of each material are summarized in Figure 4b. For MEH-PPV, the E_{ICT-} level is too high to be detected. As a result, the energy-level alignment across MEH-PPV/Al and MEH-PPV/PFN/Al is the VLA type, confirming the energy-level depiction in Figure 3a. For $PC_{71}BM$, the low E_{ICT-} level (–4.2 eV) is in agreement with the reported value measured by UPS,[40] and in perfect match with the measured effective cathode WF of ~$PC_{71}BM$/Al and ~$PC_{71}BM$/PFN/Al. For blended films of PCDTBT:$PC_{71}BM$ and PTB7:$PC_{71}BM$, the E_{ICT-} is provided by the fullerene while the E_{ICT+} comes from the donor. Therefore, the energy-level alignment across the active layer/PFN/Al in OPV devices is determined by the fullerene. The ICT levels in the blended films justify that the study of the peeled-off bilayer device (Figure 3c) can be transferred to a bulk heterojunction device.

2.5. PFN Functionality in Devices

Combining all the results, the energy-level diagrams of the regular OLED and OPV devices are plotted in **Figure 5**. In OLED

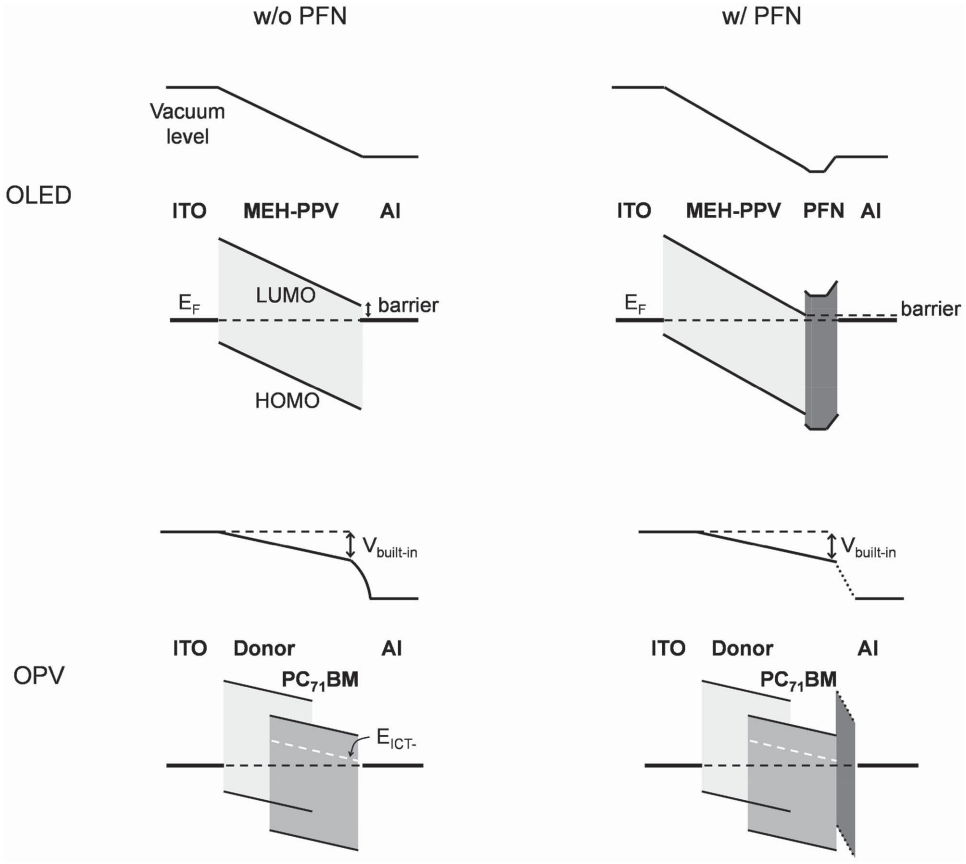

Figure 5. Energy-level diagrams of OLED and OPV devices with and without the CIM layer. The OLED's active layer is MEH-PPV, and the OPV's active layer is donor: PC71BM heterojunction (under dark condition).

devices, without PFN layer, the WF of Al is not small enough to pin to the E_{ICT-} level of MEH-PPV. Therefore, there is a large electron injection barrier at the MEH-PPV/Al interface, preventing the electron from injecting into the light-emitting layer. With PFN layer, two dipole layers with opposite direction are formed, respectively, at the MEH-PPV/PFN interface and the PFN/Al interface. Since the dipole at the PFN/Al interface is stronger than the dipole at the MEH-PPV/PFN interface, the net dipole is negative, which elevates the vacuum level of Al. As a result, the electron injection barrier is reduced, which facilitates the electron injection, thereby enhancing the device performance. Besides the dipole mechanism, hole-blocking and hole-trapping properties of PFN are also proposed to make the electron injection more efficient.[43]

For OPV devices, without PFN layer, the WF of Al pins to the fullerene E_{ICT-} forming an ohmic contact. With PFN layer, the cathode WF still pins to the fullerene E_{ICT-} level. As a consequence, the built-in potential in the active layer bulk does not change (under the dark condition). From this perspective, it is hard to understand the commonly observed better performance from the devices with PFN. Various mechanisms other than the dipole effect have been proposed to explain the improvement of the device efficiency, such as fullerene n-doping,[34,35] solvent effect,[44–47] hole-blocking/hole-trapping effect of amines,[48,49] as well as the protection of the active layer from the metal bombardment during cathode evaporation.[6]

3. Conclusion

In summary, a simple peel-off method has been developed to investigate the energy-level alignment across the organic thin-film devices. It is found that a strong negative dipole layer is formed at the PFN/Al interface, and a weak positive dipole layer is formed at the MEH-PPV/PFN interface. With a thick PFN layer as in the OLED device, the two dipole layers with opposite direction at different surfaces of the PFN layer are maintained after device fabrication. Since the WF of Al is not low enough to pin to the E_{ICT-} level of MEH-PPV, the net negative dipole across the PFN layer elevates the vacuum level on the cathode side, which reduces the electron injection barrier. As a result, the electron injection is more efficient with the PFN layer in OLED devices, thereby enhancing the device performance.

With a very thin PFN layer as in the OPV device, due to the diffusion of the Al atoms, the interface is believed to be a mixture of metal, PFN and fullerene. There is probably a competition between the PFN–Al interaction and the fullerene–PFN interaction. However, since Al WF is low enough to form the Fermi-level pinning to fullerene, any dipole at the PFN layer is screened by the spontaneous integer charge transfer caused by the pinning. Therefore, from the perspective of energy-level alignment, the modification of PFN does not introduce any significant change to the device.

The clear interpretation of the energy-level alignment across the organic electronic devices helps not only deepen the understanding of the device operation but also guide the device architecture design to achieve better performance.

Supporting Information

Supporting Information is available from the Wiley Online Library or from the author.

Acknowledgements

The authors are deeply grateful to the Ministry of Science and Technology (973 Program 2015CB655000) and the National Nature Science Foundation of China (51373057) for their financial supports.

Received: August 14, 2015
Revised: September 29, 2015
Published online: November 19, 2015

[1] C. W. Tang, S. A. VanSlyke, *Appl. Phys. Lett.* **1987**, *51*, 913.
[2] G. Horowitz, *Adv. Mater.* **1998**, *10*, 365.
[3] G. Yu, J. Gao, J. C. Hummelen, F. Wudl, A. J. Heeger, *Science* **1995**, *270*, 1789.
[4] S. Braun, W. R. Salaneck, M. Fahlman, *Adv. Mater.* **2009**, *21*, 1450.
[5] H. Ishii, K. Sugiyama, E. Ito, K. Seki, *Adv. Mater.* **1999**, *11*, 605.
[6] J. Birgerson, M. Fahlman, P. Bröms, W. R. Salaneck, *Synth. Met.* **1996**, *80*, 125.
[7] M. Jørgensen, K. Norrman, F. C. Krebs, *Sol. Energy Mater. Sol. Cells* **2008**, *92*, 686.
[8] F. Huang, H. Wu, Y. Cao, *Chem. Soc. Rev.* **2010**, *39*, 2500.
[9] H. Kang, S. Hong, J. Lee, K. Lee, *Adv. Mater.* **2012**, *24*, 3005.
[10] C. Min, C. Shi, W. Zhang, T. Jiu, J. Chen, D. Ma, J. Fang, *Angew. Chem Int. Ed.* **2013**, *52*, 3417.
[11] Y. Zhou, C. Fuentes-Hernandez, J. Shim, J. Meyer, A. J. Giordano, H. Li, P. Winget, T. Papadopoulos, H. Cheun, J. Kim, M. Fenoll, A. Dindar, W. Haske, E. Najafabadi, T. M. Khan, H. Sojoudi, S. Barlow, S. Graham, J.-L. Brédas, S. R. Marder, A. Kahn, B. Kippelen, *Science* **2012**, *336*, 327.
[12] F. Liu, Z. A. Page, V. V. Duzhko, T. P. Russell, T. Emrick, *Adv. Mater.* **2013**, *25*, 6868.
[13] H. Wang, P. Amsalem, G. Heimel, I. Salzmann, N. Koch, M. Oehzelt, *Adv. Mater.* **2013**, *26*, 925.
[14] J. H. Kim, Y. E. Ha, G. E. Lim, M. Y. Jo, J. Park, Y.-C. Kang, S.-J. Moon, *J. Mater. Chem. C* **2014**, *2*, 3820.
[15] Z.-G. Zhang, B. Qi, Z. Jin, D. Chi, Z. Qi, Y. Li, J. Wang, *Energy Environ. Sci.* **2014**, *7*, 1966.
[16] W.-Y. Tan, R. Wang, M. Li, G. Liu, P. Chen, X.-C. Li, S.-M. Lu, H. L. Zhu, Q.-M. Peng, X.-H. Zhu, W. Chen, W. C. H. Choy, F. Li, J. Peng, Y. Cao, *Adv. Funct. Mater.* **2014**, *24*, 6540.
[17] Z. He, C. Zhong, X. Huang, W.-Y. Wong, H. Wu, L. Chen, S. Su, Y. Cao, *Adv. Mater.* **2011**, *23*, 4636.
[18] S.-N. Hsieh, S.-W. Hsiao, T.-Y. Chen, C.-Y. Li, C.-H. Lee, T.-F. Guo, Y.-J. Hsu, T.-L. Lin, Y. Wei, T.-C. Wen, *J. Mater. Chem.* **2011**, *21*, 8715.
[19] H. Wang, W. Zhang, C. Xu, X. Bi, B. Chen, S. Yang, *ACS Appl. Mater. Interfaces* **2012**, *5*, 26.
[20] X. Ouyang, R. Peng, L. Ai, X. Zhang, Z. Ge, *Nat. Photonics* **2015**, *9*, 520.
[21] W. R. Salaneck, J.-L. Brédas, *Adv. Mater.* **1996**, *8*, 48.
[22] W. Osikowicz, M. P. de Jong, S. Braun, C. Tengstedt, M. Fahlman, W. R. Salaneck, *Appl. Phys. Lett.* **2006**, *88*, 193503.
[23] S. van Reenen, S. Kouijzer, R. A. J. Janssen, M. M. Wienk, M. Kemerink, *Adv. Mater. Interfaces* **2014**, *1*, 1400189.
[24] Z. Jiang, Z. Zhong, S. Xue, Y. Zhou, Y. Meng, Z. Hu, N. Ai, J. Wang, L. Wang, J. Peng, Y. Ma, J. Pei, J. Wang, Y. Cao, *ACS Appl. Mater. Interfaces* **2014**, *6*, 8345.
[25] Z. He, B. Xiao, F. Liu, H. Wu, Y. Yang, S. Xiao, C. Wang, T. P. Russell, Y. Cao, *Nat. Photonics* **2015**, *9*, 174.

[26] Z. He, C. Zhong, S. Su, M. Xu, H. Wu, Y. Cao, *Nat. Photonics* **2012**, *6*, 591.
[27] J. Park, R. Yang, C. V. Hoven, A. Garcia, D. A. Fischer, T.-Q. Nguyen, G. C. Bazan, D. M. DeLongchamp, *Adv. Mater.* **2008**, *20*, 2491.
[28] R. Schlapak, D. Armitage, N. Saucedo-Zeni, G. Latini, H. J. Gruber, P. Mesquida, Y. Samotskaya, M. Hohage, F. Cacialli, S. Howorka, *Langmuir* **2007**, *23*, 8916.
[29] C. Fauquet, P. Dubot, L. Minel, M.-G. Barthés-Labrousse, M. Rei Vilar, M. Villatte, *Appl. Surf. Sci.* **1994**, *81*, 435.
[30] M. Lv, S. Li, J. J. Jasieniak, J. Hou, J. Zhu, Z. Tan, S. E. Watkins, Y. Li, X. Chen, *Adv. Mater.* **2013**, *25*, 6889.
[31] A. Vilan, J. Ghabboun, D. Cahen, *J. Phys. Chem. B* **2003**, *107*, 6360.
[32] K. Zhang, C. Zhong, S. Liu, C. Mu, Z. Li, H. Yan, F. Huang, Y. Cao, *ACS Appl. Mater. Interfaces* **2014**, *6*, 10429.
[33] S. Liu, K. Zhang, J. Lu, J. Zhang, H.-L. Yip, F. Huang, Y. Cao, *J. Am. Chem. Soc.* **2013**, *135*, 15326.
[34] C.-Z. Li, C.-C. Chueh, F. Ding, H.-L. Yip, P.-W. Liang, X. Li, A. K.-Y. Jen, *Adv. Mater.* **2013**, *25*, 4425.
[35] S. Fabiano, S. Braun, X. Liu, E. Weverberghs, P. Gerbaux, M. Fahlman, M. Berggren, X. Crispin, *Adv. Mater.* **2014**, *26*, 6000.
[36] K. Zhang, Z. Hu, R. Xu, X.-F. Jiang, H.-L. Yip, F. Huang, Y. Cao, *Adv. Mater.* **2015**, *27*, 3607.
[37] C. Schwarz, F. Milan, T. Hahn, M. Reichenberger, S. Kümmel, A. Köhler, *Adv. Funct. Mater.* **2014**, *24*, 6439.
[38] P. Sehati, S. Braun, L. Lindell, X. Liu, L. M. Andersson, M. Fahlman, *IEEE J. Sel. Top. Quantum Electron* **2010**, *16*, 1718.
[39] C. J. Brabec, a. Cravino, D. Meissner, N. S. Sariciftci, T. Fromherz, M. T. Rispens, L. Sanchez, J. C. Hummelen, *Adv. Funct. Mater.* **2001**, *11*, 374.
[40] Q. Bao, O. Sandberg, D. Dagnelund, S. Sandén, S. Braun, H. Aarnio, X. Liu, W. M. Chen, R. Österbacka, M. Fahlman, *Adv. Funct. Mater.* **2014**, *24*, 6309.
[41] W. Ma, P. K. Iyer, X. Gong, B. Liu, D. Moses, G. C. Bazan, A. J. Heeger, *Adv. Mater.* **2005**, *17*, 274.
[42] E. L. Ratcliff, J. Meyer, K. X. Steirer, N. R. Armstrong, D. Olson, A. Kahn, *Org. Electron.* **2012**, *13*, 744.
[43] Z. Zhong, Z. Hu, Z. Jiang, J. Wang, Y. Chen, C. Song, S. Han, F. Huang, J. Peng, J. Wang, Y. Cao, *Adv. Electron. Mater.* **2015**, *1*, 1400014.
[44] H. Zhou, Y. Zhang, J. Seifter, S. D. Collins, C. Luo, G. C. Bazan, T.-Q. Nguyen, A. J. Heeger, *Adv. Mater.* **2013**, *25*, 1646.
[45] A. Kumar, G. Lakhwani, E. Elmalem, W. T. S. Huck, A. Rao, N. C. Greenham, R. H. Friend, *Energy Environ. Sci.* **2014**, *7*, 2227.
[46] L. Ye, Y. Jing, X. Guo, H. Sun, S. Zhang, M. Zhang, L. Huo, J. Hou, *J. Phys. Chem. C* **2013**, *117*, 14920.
[47] Z. Xiao, Y. Yuan, B. Yang, J. VanDerslice, J. Chen, O. Dyck, G. Duscher, J. Huang, *Adv. Mater.* **2014**, *26*, 3068.
[48] C. Duan, W. Cai, B. B. Y. Hsu, C. Zhong, K. Zhang, C. Liu, Z. Hu, F. Huang, G. C. Bazan, A. J. Heeger, Y. Cao, *Energy Environ. Sci.* **2013**, *6*, 3022.
[49] W. Cai, C. Zhong, C. Duan, Z. Hu, S. Dong, D. Cao, M. Lei, F. Huang, Y. Cao, *Appl. Phys. Lett.* **2015**, *106*, 4922467.